An X-ray FEL-based $\gamma\gamma$ Collider Higgs Factory - Material for AF03 Summary Report

Tim Barklow[1,a], Zhirong Huang[1], Adham Naji[1], Emilio Nanni[1], James Rosenzweig[2], Anne Sakdinawat[1], Sami Tantawi[1], and Glen White[1]

[1]SLAC Linear Accelerator Center, Stanford, Menlo Park, CA
[2]Particle Beam Physics Laboratory, University of California Los Angeles, CA
[a]timb@slac.stanford.edu

December 16, 2020

To date, most $\gamma\gamma$ collider Higgs factory designs have utilized optical wavelength lasers. The center-of-mass energy of the electron–photon system is usually constrained to $x < 4.82$, where $x = 4E_e\omega_0/m_e^2$, m_e is the electron mass and E_e (ω_0) is the electron (laser photon) energy. Larger x values are problematic due to the (linear QED) thresholds of $x = 4.82$ ($x = 8.0$) for the processes $\gamma\gamma_0 \to e^+e^-$ ($e^-\gamma_0 \to e^-e^+e^-$), where γ and γ_0 refer to the Compton-scattered and laser photon, respectively. Larger x values, however, also carry advantages. As x is increased the $\gamma\gamma$ luminosity distribution with respect to center-of-mass energy is more sharply peaked near the maximum center-of-mass energy value. Such a distribution increases the production rate of a narrow resonance relative to $\gamma\gamma$ background processes when the peak is tuned to the resonance mass. This report describes the design of a $\gamma\gamma$ Higgs factory with $x = 1000$, in which 63 GeV electron beams collide with 1 keV X-ray free electron laser (XFEL) beams. The Higgs boson production rate for this collider is 30,000 Higgs bosons per (10^7 second) year, roughly the same as the ILC Higgs rate.

1 Design Outline

1.1 Higgs Factory Configuration

A schematic of the $\gamma\gamma$ collider is shown in Fig. 1. While the Snowmass Letter of Intent (LOI) indicated four linear electron accelerators (LINAC's), the current design makes do with two. An RF gun produces 90% polarized electrons with 0.62×10^{10} electrons per bunch and 76 bunches per train at a repetition rate of 240 Hz. The normalized horizontal and vertical emittances out of the gun are 0.12 microns each. The Cool Copper Collider (C^3)[1] LINAC accelerates the electron bunches with a bunch spacing of 2 ns and a gradient of 100 MeV/m. At the 31 GeV point every other bunch is diverted to the XFEL line where a helical undulator produces circular polarized 1 keV X-ray light with 0.7 Joules per pulse. The remaining bunches continue down the LINAC until reaching an energy of 62.8 GeV, after which they pass through a final focus section that squeezes the geometric horizontal and vertical spot sizes to 5.4 nm at the primary e^-e^- interaction point (IP). The e^-e^- geometric luminosity is $9.7 \times 10^{34}\text{cm}^2\ \text{s}^{-1}$. At 100 microns upstream of the primary IP, the 62.8 GeV electrons collide with the X-ray laser light from the opposing XFEL line to produce 62.5 GeV photons. The X-ray light has been focused at this point from 10 microns at the end of the XFEL to a waist radius of a_γ=40 nm using Kirkpatrick-Baez (KB) mirrors.

The distribution of $\gamma\gamma$ luminosity versus $\gamma\gamma$ center-of-mass energy $E_{\gamma\gamma}$ as calculated with the CAIN Monte Carlo[2] is shown in Fig. 2 for $2P_c\lambda_e = +0.9$, where $P_c = +1$ and $\lambda_e = +0.45$ are the helicities of the laser photon and electron, respectively. Also shown for comparison is the corresponding distribution from an x=4.82 optical laser $\gamma\gamma$ collider with $2P_c\lambda_e = -0.9$. The distribution for x=1000 has a single asymmetric peak at the Higgs boson mass with widths of 2.1 GeV (0.3 GeV) on the low (high) side of the peak, and no other structure. In contrast, the $x = 4.82$ distribution has a peak at the Higgs boson mass with widths of 22.0 GeV (5.6 GeV) on the low (high) side plus additional structure at lower $\gamma\gamma$ center-of-mass energies.

It is clear from Fig.2 that the background to Higgs production from $\gamma\gamma$ annihilation processes is much reduced at $x = 1000$ with respect to $x = 4.82$. However, the physics environment is not background-free. Luminosities for the e^-e^-, $e^-\gamma$, $\gamma\gamma$, and e^+e^- initial states are given in Table1. Backgrounds that need to be considered include $e^-\gamma \to e^-Z$ and $e^+e^- \to \gamma Z$.

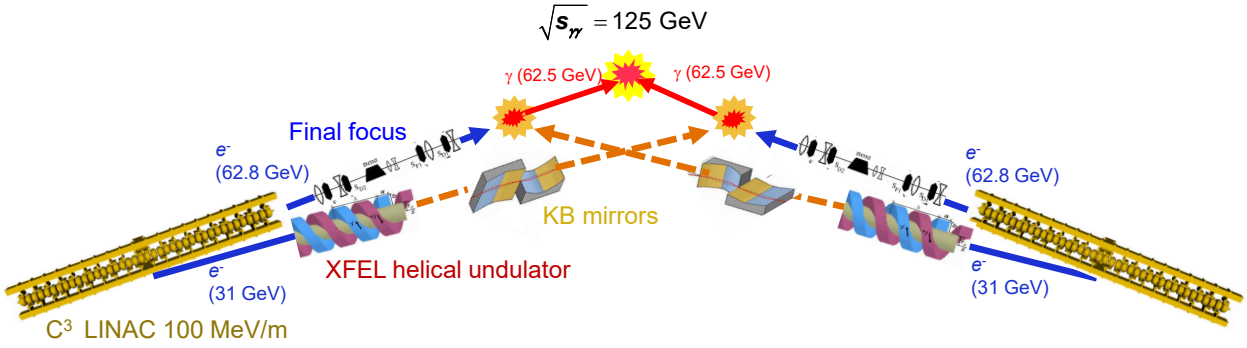

Figure 1: Schematic of X-ray FEL-based gamma gamma Collider Higgs Factory.

Table 1: Summary of Compton and Primary IP parameters.

	x=1000 $2P_c\lambda_e = +0.9$	x=1000 $2P_c\lambda_e = -0.9$
Laser wavelength λ (nm)	1.2	1.2
Laser waist radius a_γ (nm)	37.7	37.7
Laser pulse length $= 2\beta_\gamma = \frac{4\pi a_\gamma^2}{\lambda}$ (μm)	15.0	15.0
Laser pulse energy (J)	0.72	0.72
e^- Compton conversion efficiency (%)	44.2	37.1
peak non-linear QED $\xi^2 = \frac{2n_\gamma r_e^2 \lambda}{\alpha}$	0.17	0.17
$\mathcal{L}_{\gamma\gamma}$ (10^{33} cm^{-2} s^{-1})	0.92	0.13
$\mathcal{L}_{e^-\gamma}$	6.21	2.4
$\mathcal{L}_{e^+\gamma}$	0.54	0.24
$\mathcal{L}_{e^-e^-}$	7.5	8.0
$\mathcal{L}_{e^+e^-}$	2.54	3.64
$\mathcal{L}_{e^+e^-}$, $\sqrt{s} > 50$ GeV	0.34	0.38
$N_{\rm Higgs}$/yr	30,800	21,700
$\Delta\Gamma_H$ from 1 yr energy scan (MeV)	34	8

The helicity combination $2P_c\lambda_e = +0.9$ is chosen to maximize the Higgs boson production rate. When measuring the Higgs width with an energy scan about the Higgs resonance it is better to use $2P_c\lambda_e = -0.9$, as shown in Fig. 3. The Higgs production rate with $2P_c\lambda_e = -0.9$ is 70% of the rate with $2P_c\lambda_e = +0.9$, but the leading edge width of the peak in the luminosity distribution is five times smaller at 70 MeV. A dedicated one year energy scan would yield a Higgs width measurement precision of 8 MeV, just a factor of two away from the Standard Model Higgs width value of 4 MeV. The width of the peak in the luminosity distribution for $2P_c\lambda_e = -0.9$ is dominated by the electron beam energy spread, so that the Higgs width measurement could be improved further by reducing the electron beam energy spread below 0.05%.

Scans of the r.m.s. electron longitudinal bunch density and the XFEL beam waist radius are shown in Fig. 4. In addition to illustrating the sensitivity of the luminosity to electron bunch length and laser waist, the plots also demonstrate the impact of different Compton processes on the luminosity. Note the large effect from the Bethe-Heitler process $e^-\gamma_0 \to e^-e^+e^-$.

1.2 Electron Accelerator

The C^3 technology represents a new methodology for dramatically reducing the cost of high gradient accelerators, while increasing their capabilities in terms of gradient and efficiency. After two decades of exploring the high gradient phenomena observed in room-temperature accelerator structures, we have been able to deduce the underlying physics models related to these phenomena. This knowledge led us to create a new paradigm for the design of

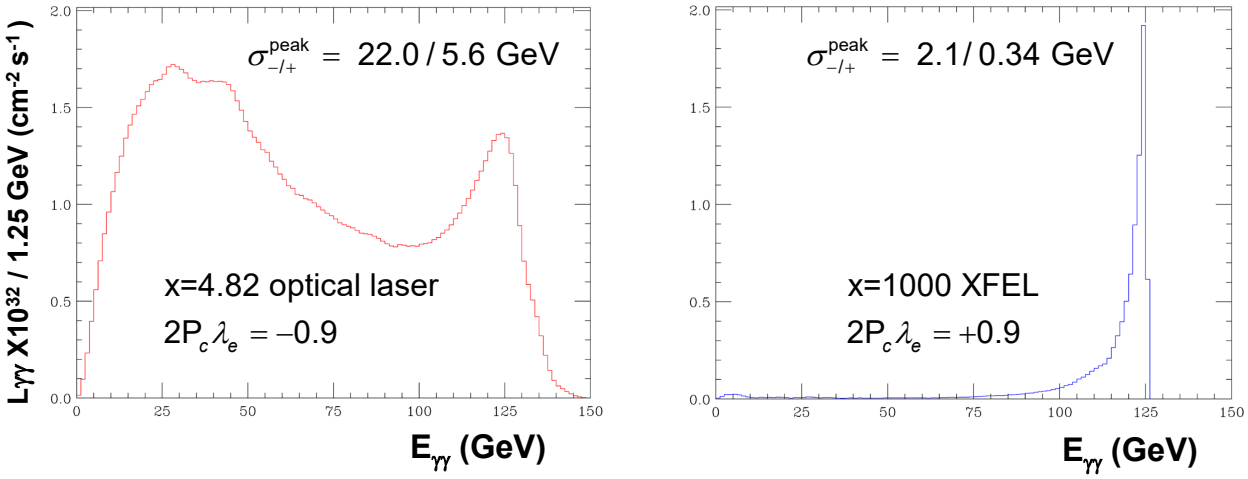

Figure 2: $\gamma\gamma$ luminosity versus $\gamma\gamma$ center-of-mass energy $E_{\gamma\gamma}$ for x=4.82 & $2P_c\lambda_e = -0.9$ (left) and x=1000 & $2P_c\lambda_e = +0.9$ (right) as calculated by the CAIN MC, where P_c and λ_e are the helicities of the laser photon and electron, respectively. The 0.05% electron beam energy spread, linear QED Bethe Heitler scattering and non-linear QED effects in Compton and Breit-Wheeler scattering are included in the CAIN simulation. The asymmetric widths of the peaks in the distributions at $E_{\gamma\gamma}$=125 GeV are indicated.

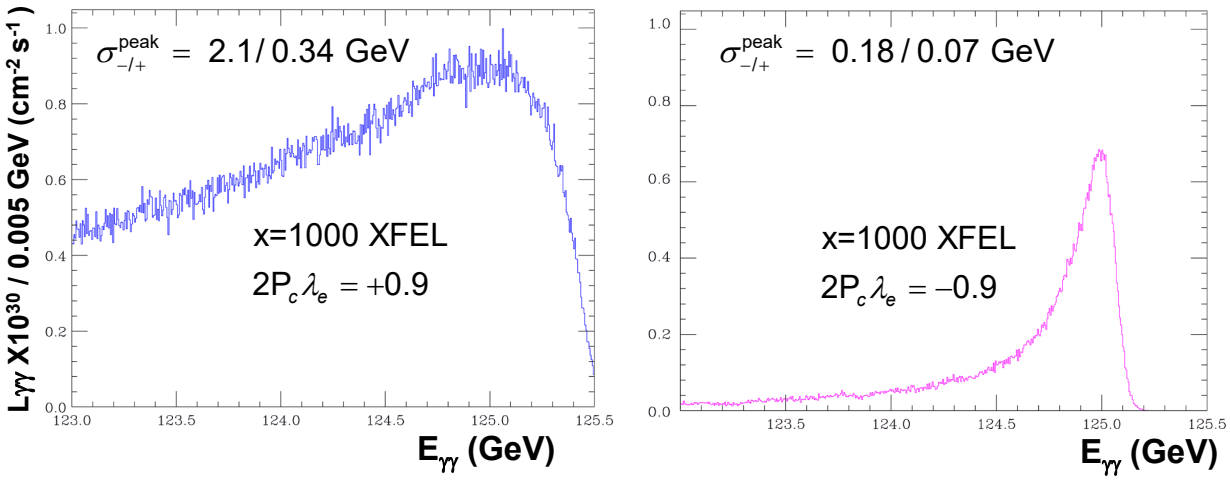

Figure 3: $\gamma\gamma$ luminosity versus $\gamma\gamma$ center-of-mass energy $E_{\gamma\gamma}$ for x=1000 & $2P_c\lambda_e = +0.9$ (left) and x=1000 & $2P_c\lambda_e = -0.9$ (right) as calculated by the CAIN MC, where P_c and λ_e are the helicities of the laser photon and electron, respectively. The 0.05% electron beam energy spread, linear QED Bethe Heitler scattering and non-linear QED effects in Compton and Breit-Wheeler scattering are included in the CAIN simulation. The asymmetric widths of the peaks in the distributions at $E_{\gamma\gamma}$=125 GeV are indicated. Note that the 5 MeV bin size is close to the Standard Model Higgs width of 4 MeV.

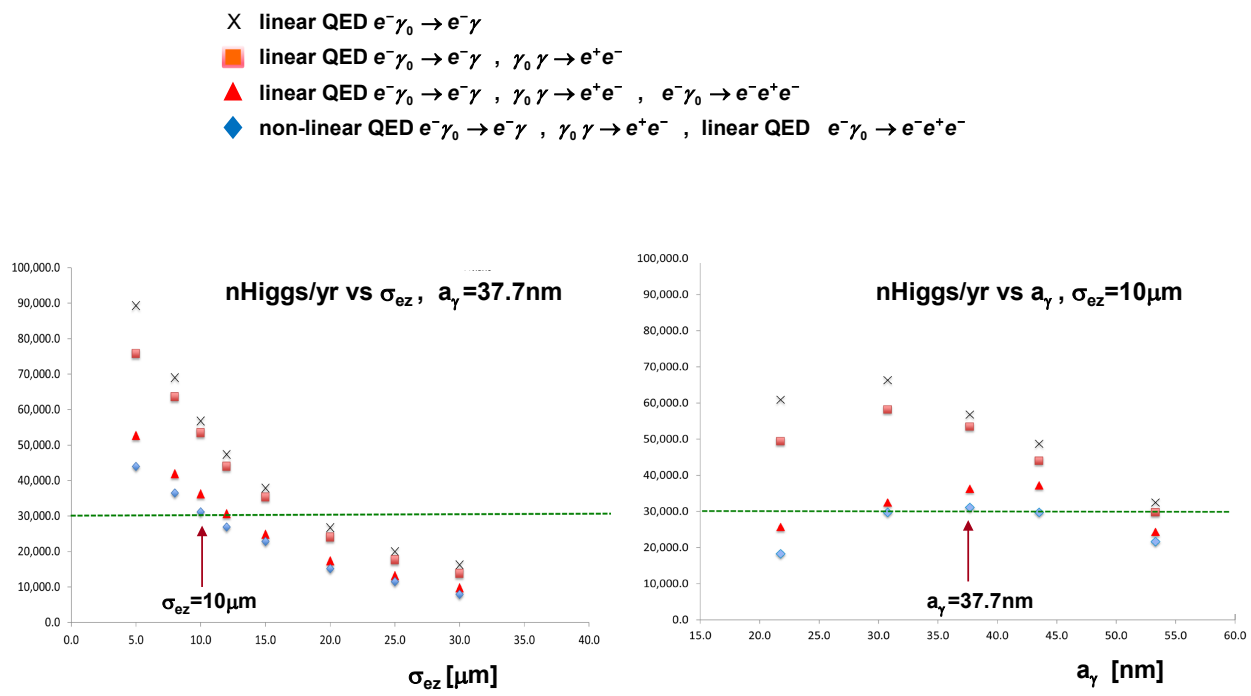

Figure 4: Scans of the r.m.s. electron longitudinal bunch density σ_{ez} and the waist radius a_γ of the XFEL beam at the Compton interaction point (IP), showing the impact of different Compton IP processes on the $\gamma\gamma$ luminosity. In the expressions for the Compton IP processes the symbols γ_0 and γ refer to laser photon and scattered photon, respectively.

accelerator structures, which includes: a new topology for the structure geometry [3, 4] operating at cryogenic temperature [5], the use of doped copper in the construction of these structures [6], and a new methodology for the selection of operating frequency bands [6]. In particular, for science discovery machines, optimization exercises have revealed that the optimal frequency should be around 6–8 GHz for operation with a gradient well above 100 MV/m while maintaining exquisite beam parameters. That explains why both UCLA and LANL are trying very hard to build their infrastructure at C-band (5.721 GHz), a frequency band that is close enough to the optimal point, but with some industrial support behind it.

Furthermore, the so-called "distributed-coupling structure" [3] and its operation at cryogenic temperature represent a breakthrough for the e^- source. Electron guns can be designed around this concept with an unprecedented brightness [7]. Using this technology can result in an extremely economical system for this γ-γ collider. The two linacs required for the collider could be made extremely compact due to the high gradient capabilities of the C^3 technology and the limited energy reach required of 62.5 GeV. With the bright electron beam sources, we could also eliminate the damping rings. An example parameter set is discussed below.

1.3 X-ray FEL

The two identical X-ray FEL lines, which provide the necessary circularly-polarized 1.2 nm (1 keV) photons, can be constructed using a long helical undulator. Due to the high magnetic field and high electron energy considered here, the quantum diffusion energy spread in such an undulator must be taken into account and properly included in design calculations. As the main linac can accelerate electrons to 62.5 GeV, we take the electron energy for the XFEL line to be around 31 GeV, with normalized emittance of 120 nm, bunch charge of 1 nC and relative RMS slice energy spread of $\langle\Delta\gamma/\gamma\rangle$ of 0.05%.

Using a permanent-magnet undulator, with peak magnetic field slightly above 1 Tesla, undulator period around 9 cm and an average β-function of 12 m, we can produce 1 keV X-ray pulse energy $\sim$ 0.07 J at FEL saturation length of roughly 60 m and with negligible quantum diffusion effects [8, 9]. As we know from a decade of X-ray FEL studies, if we can produce a seeded FEL (such as through self-seeding or other similar processes) and taper the undulator's K parameter after saturation, we can continue to extract X-ray pulse energy with an order-of-magnitude improvement in efficiency [10]. Then we can reach the targeted pulse energy of 0.7 J at 1 keV photon energy, which is about 2.3% of the electron beam energy. The overall length of the undulators is estimated to be within 200 m. This is just an example parameter set (summarized in Table 2 below). Detailed optimization and

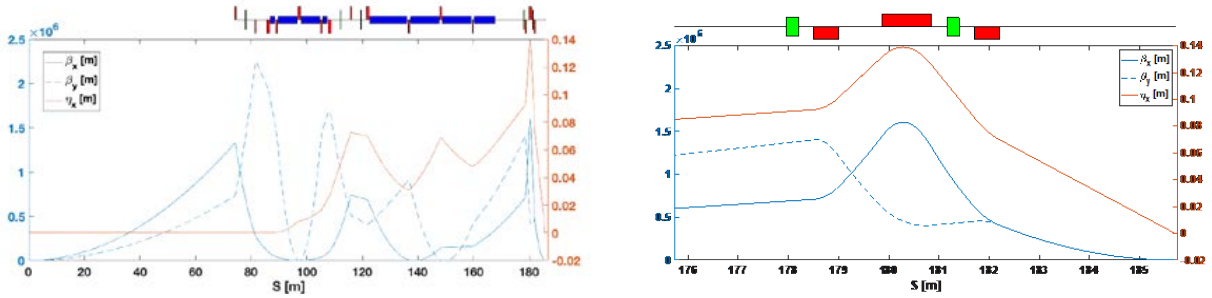

Figure 5: Beta and horizontal dispersion functions for final focus beamline (IP is on the right). The right figure shows a close up of the IP triplet.

simulation studies will be reported elsewhere.

Table 2: Summary of approximate design parameters.

Final Focus parameters	Approx. value	XFEL parameters	Approx. value
Electron energy	62.8 GeV	Electron energy	31 GeV
β_x/β_y	0.03/0.03 mm	normalized emittance	120 nm
$\gamma\epsilon_x/\gamma\epsilon_y$	120/120 nm	RMS energy spread $\langle\Delta\gamma/\gamma\rangle$	0.05%
σ_x/σ_y at e^-e^- IP	5.4/5.4 nm	bunch charge	1 nC
σ_z	10 μm	Undulator B field	$\gtrsim 1$ T
bunch charge	1 nC	Undulator period λ_u	9 cm
Rep. Rate at IP	240×36 Hz	Average β function	12 m
σ_x/σ_y at Compton IP	18.8/18.8 nm	x-ray λ (energy)	1.2 nm (1 keV)
$\mathcal{L}_{\text{geometric}}$	9.7×10^{34} cm^2 s^{-1}	x-ray pulse energy	0.7 J
δ_E/E	0.05%		
L^* (Q0 exit to e^- IP)	3.5m		
$\eta_x'^*$	20 mrad		
magnet aperture	2 cm diameter		

1.4 Final Focus

A preliminary layout for the final focus system is shown below in Fig. 5. This is not an optimized design at this stage and is shown for illustration purposes only. The length of the system is about 110m as shown, using realistic magnet strengths. The design follows that used for ILC and CLIC, namely the local chromatic compensation scheme proposed by Raimondi & Seryi[11] and tested at ATF2, KEK[12]. The design uses a pair of sextupole magnets located locally to the final triplet to cancel the chromaticity generated by the final focus system magnets. An interleaved, second pair of sextupoles are used to simultaneously cancel geometric aberrations introduced by the chromatic correction sextupoles, with a fifth sextupole used to help control third-order aberrations generated by the interleaved sextupole pairs. Octupoles, decupoles (and perhaps higher harmonic magnets) will also be required but are not shown here. Horizontal dispersion, required for the chromatic cancelation to occur, is generated by three families of bend magnets. The length of the bend magnets is chosen such that negligible emittance growth due to synchrotron radiation exists.

2 Readiness

The overall geometric layout of the accelerator, XFEL, X-ray focusing and final focus lines is under study.

2.1 RF Electron Gun

2.2 Accelerator

2.3 XFEL

2.4 X-ray Optics

The damage threshold of the KB mirrors is being investigated.

2.5 Final Focus

The final focus design differs from than that of ILC & CLIC in 2 key aspects, each of which raises concerns which need further studies to address:

- Round beams at the IP leads to the preference of a final triplet instead of final doublet configuration. The required angular dispersion at the IP is about double that required for ILC/CLIC to achieve the same dispersion at the sextupole locations. This will have an adverse effect on the momentum acceptance of the extraction line and may lead to increased detector backgrounds.
- The requested IP beta functions are 0.03 mm in both planes. This should be compared with 11 x 0.48 mm for the baseline ILC design (and a corresponding design tested at the ATF2 facility). The much smaller β^* values here generate significantly higher chromatic distortions, requiring stronger sextupole corrections. This in turn requires more finely tuned 3rd, 4th+ order corrections to compensate for the sextupoles. Experience from CLIC tuning studies and operational experience at ATF2 has shown that tolerances become rapidly tighter (magnet field quality and positional tolerances) as β^* is lowered below ILC values, and online tuning becomes harder and takes longer. Also, operational experience at ATF2 showed that tuning becomes more difficult with smaller $\beta_x^* : \beta_y^*$ ratios (where the smallest spot sizes were only accomplished at 10X design β_x^*). With this in mind, a careful study of the tolerances of this, modified, final focus design is important to understand the ramifications on expected delivered luminosity.

2.6 Machine Detector Interface

Detector background from the low energy photons, electrons and positrons produced at the Compton IP is a concern, and will be studied with the CAIN Monte Carlo.

3 Similar existing technology

4 State of the Technical Design Report

5 State of Proposal

6 Proposals for upgrades or extensions

6.1 Luminosity Upgrades

7 Stageability to future experiments

References

[1] Karl L. Bane et al. "An Advanced NCRF Linac Concept for a High Energy e^+e^- Linear Collider". In: (July 2018). arXiv: 1807.10195 [physics.acc-ph].

[2] P. Chen et al. "CAIN: Conglomerat d'ABEL et d'interactions nonlineaires". In: *Nucl. Instrum. Meth. A* 355 (1995), pp. 107–110. DOI: 10.1016/0168-9002(94)01186-9.

[3] Sami Tantawi et al. "Design and demonstration of a distributed-coupling linear accelerator structure". In: *Accepted for publication in Physical Review Accelerator and Beams* (2020).

[4] Valery Dolgashev et al. "Geometric dependence of radio-frequency breakdown in normal conducting accelerating structures". In: *Applied Physics Letters* 97.17 (2010), p. 171501. DOI: 10.1063/1.3505339. eprint: https://doi.org/10.1063/1.3505339. URL: https://doi.org/10.1063/1.3505339.

[5] Mamdouh Nasr. "Distributed coupling Linacs from Room Temperature to Superconducting". In: *talk at the International Linac Conference, Sep. 2020* (2020).

[6] Lisa Laurent et al. "Experimental study of rf pulsed heating". In: *Phys. Rev. ST Accel. Beams* 14 (4 Apr. 2011), p. 041001. DOI: 10.1103/PhysRevSTAB.14.041001. URL: https://link.aps.org/doi/10.1103/PhysRevSTAB.14.041001.

[7] J. B. Rosenzweig et al. "Next generation high brightness electron beams from ultrahigh field cryogenic rf photocathode sources". In: *Phys. Rev. Accel. Beams* 22 (2 Feb. 2019), p. 023403. DOI: 10.1103/PhysRevAccelBeams.22.023403. URL: https://link.aps.org/doi/10.1103/PhysRevAccelBeams.22.023403.

[8] Kwang-Je Kim, Zhirong Huang, and Ryan Lindberg. *Synchrotron Radiation and Free-Electron Lasers: Principles of Coherent X-Ray Generation*. Cambridge University Press, 2017. DOI: 10.1017/9781316677377.

[9] Zhirong Huang and Kwang-Je Kim. "Review of x-ray free-electron laser theory". In: *Phys. Rev. ST Accel. Beams* 10 (3 Mar. 2007), p. 034801. DOI: 10.1103/PhysRevSTAB.10.034801. URL: https://link.aps.org/doi/10.1103/PhysRevSTAB.10.034801.

[10] Y. Jiao et al. "Modeling and multidimensional optimization of a tapered free electron laser". In: *Phys. Rev. ST Accel. Beams* 15 (5 May 2012), p. 050704. DOI: 10.1103/PhysRevSTAB.15.050704. URL: https://link.aps.org/doi/10.1103/PhysRevSTAB.15.050704.

[11] Pantaleo Raimondi and Andrei Seryi. "A Novel final focus design for future linear colliders". In: *Phys. Rev. Lett.* 86 (2001), pp. 3779–3782. DOI: 10.1103/PhysRevLett.86.3779.

[12] G.R. White et al. "Experimental Validation of a Novel Compact Focusing Scheme for Future Energy-Frontier Linear Lepton Colliders". In: *Phys. Rev. Lett.* 112.3 (2014), p. 034802. DOI: 10.1103/PhysRevLett.112.034802.